

1 **Appendix**

2 **The Ebola virus VP40 matrix layer undergoes endosomal**
3 **disassembly essential for membrane fusion**

4 Sophie L. Winter^{1,2}, Gonen Golani^{2,3}, Fabio Lolicato^{4,5}, Melina Vallbracht^{1,2}, Keerthihan
5 Thiyagarajah^{1,2}, Samy Sid Ahmed⁶, Christian Lüchtenborg⁴, Oliver T. Fackler^{6,7}, Britta Brügger⁴,
6 Thomas Hoenen⁸, Walter Nickel⁴, Ulrich S. Schwarz^{2,3}, Petr Chlanda^{1,2*}

7 ¹ Schaller Research Groups, Department of Infectious Diseases, Virology, University Hospital Heidelberg, Heidelberg,
8 Germany

9 ² BioQuant-Centre for Quantitative Biology, Heidelberg University, Heidelberg, Germany

10 ³ Institute for Theoretical Physics, Heidelberg University, Heidelberg, Germany

11 ⁴ Heidelberg University Biochemistry Center, Heidelberg, Germany

12 ⁵ Department of Physics, University of Helsinki, Helsinki, Finland

13 ⁶ Department of Infectious Diseases, Integrative Virology, University Hospital Heidelberg, Heidelberg, Germany

14 ⁷ German Centre for Infection Research (DZIF), Partner Site Heidelberg, Germany

15 ⁸ Institute of Molecular Virology and Cell Biology, Friedrich-Loeffler-Institut, Greifswald-Insel Riems, Germany

16 *Correspondence: chlanda@bioquant.uni-heidelberg.de

17 **Table of Contents**

18 Appendix Figure S1 2

19 Appendix Figure S2 3

20 Appendix Figure S3 4

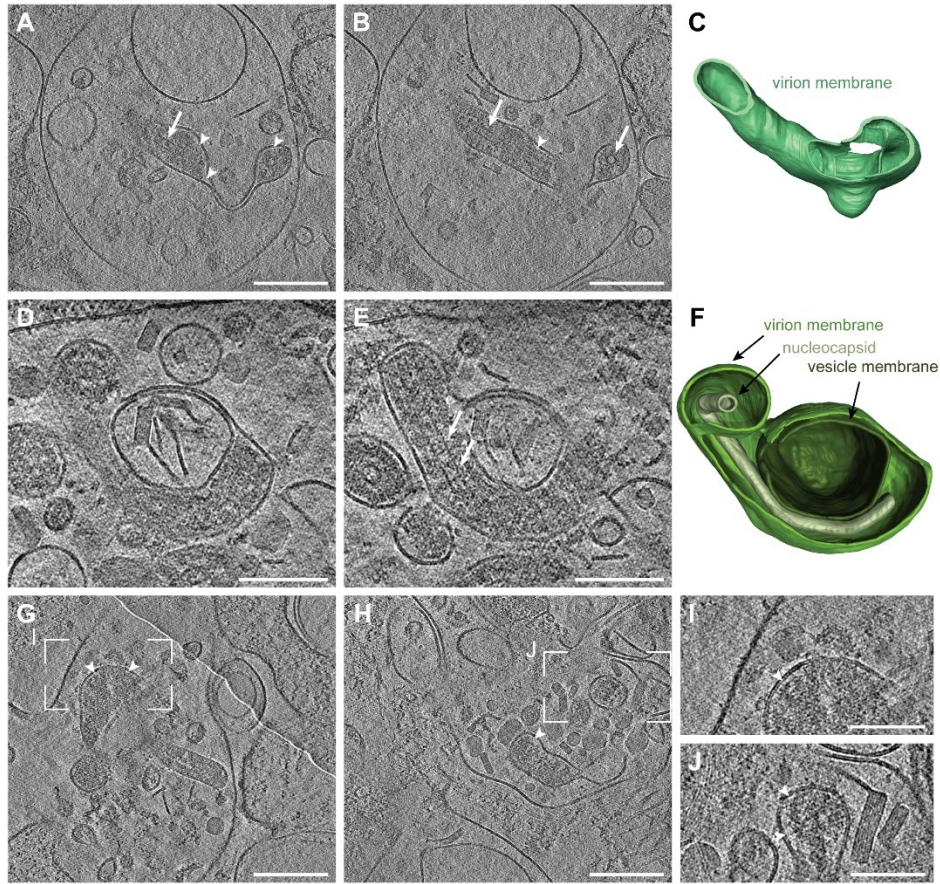
21 Appendix Figure S4 5

22 Appendix Figure S5 6

23

24

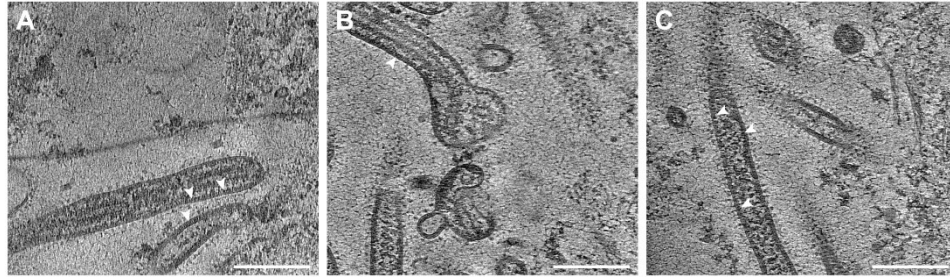
25



26

27 **Appendix Figure S1**

28 **In situ cryo-ET of EBOV infecting Huh7 cells.** Slices through tomograms showing Ebola
 29 virions inside late endosomal compartments. All virions display condensed nucleocapsids (white
 30 arrows) and disassembled VP40 layers, which have detached from the viral membrane as
 31 apparent from the gap adjacent to the inner lipid monolayer (white arrowheads). **(A-B)** Different
 32 slices through the same tomogram showing an internalized EBOV with a disassembled VP40
 33 matrix and highly flexible membrane. The nucleocapsid is still condensed (white arrow). **(C)** 3D
 34 segmentation of the lipid envelope of the EBOV virion (green) shown in (A) and (B). **(D-E)**
 35 Different slices through the same tomogram showing an internalized EBOV virion with a
 36 disassembled VP40 matrix and condensed nucleocapsid. The virion had engulfed an
 37 intraluminal vesicle containing cholesterol ester crystals, indicating that this virus has undergone
 38 fusion. **(F)** 3D segmentation of EBOV shown in (D) and (E) showing the viral membrane (green),
 39 nucleocapsid (light green) and vesicle membrane (dark green). Scale bars: (A), (B): 200 nm, (D-
 40 J): 100 nm.

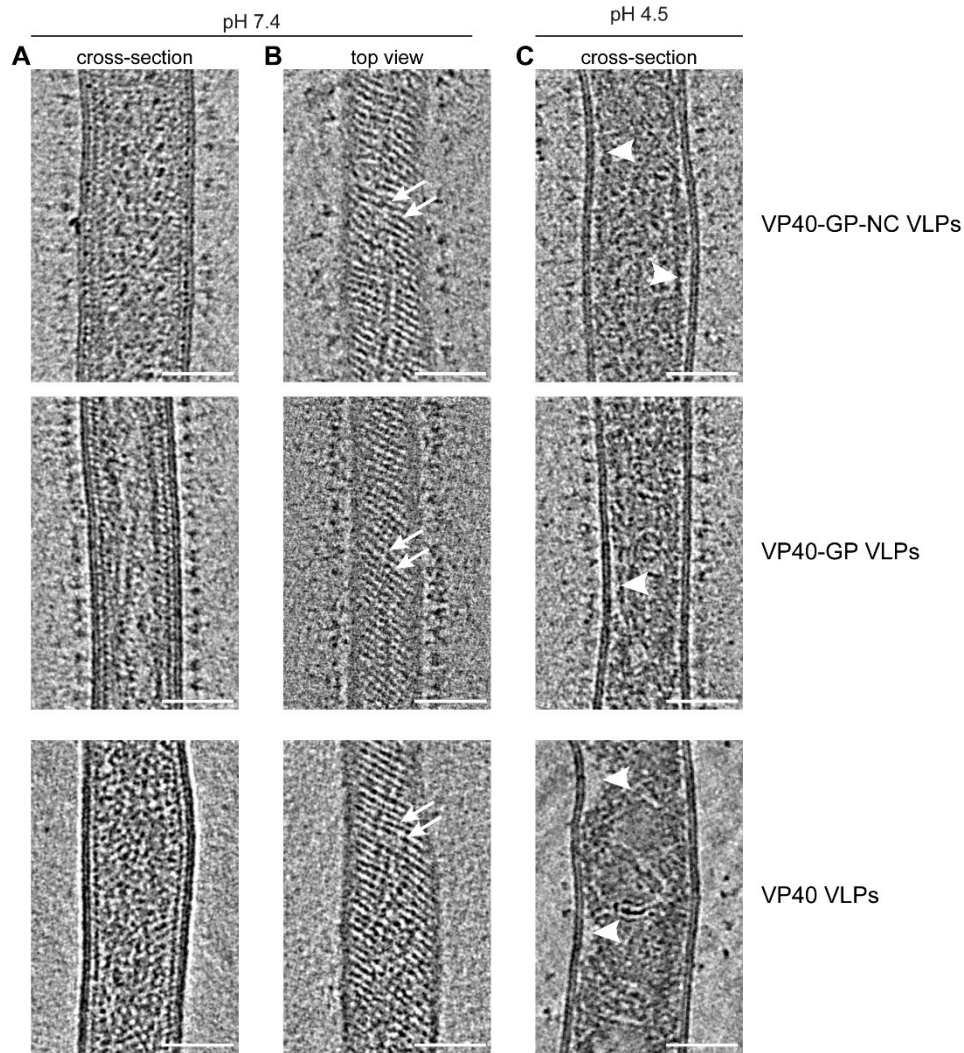


41

42 **Appendix Figure S2**

43 **In situ cryo-ET of budding and released EBOV from infecting Huh7 cells. (A-C)** Slices
44 through tomograms showing Ebola virions adjacent to the plasma membrane of infected Huh7
45 cells. All virions contain assembled VP40 layers as apparent from the regular densities
46 decorating the inner lipid monolayer at the luminal side (white arrowheads). Scale bars: 200 nm.

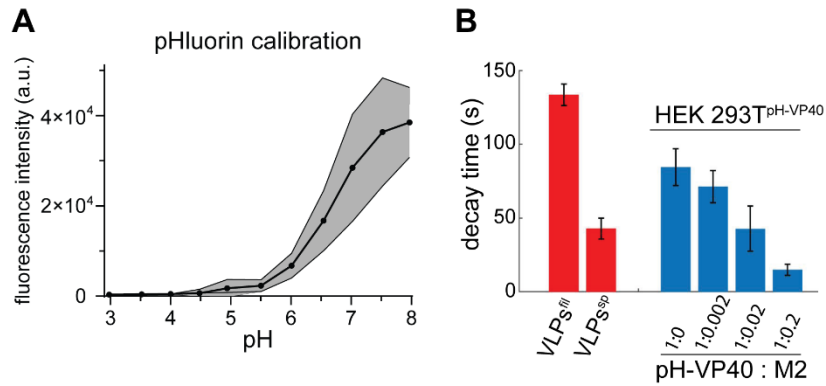
47



48

49 **Appendix Figure S3**

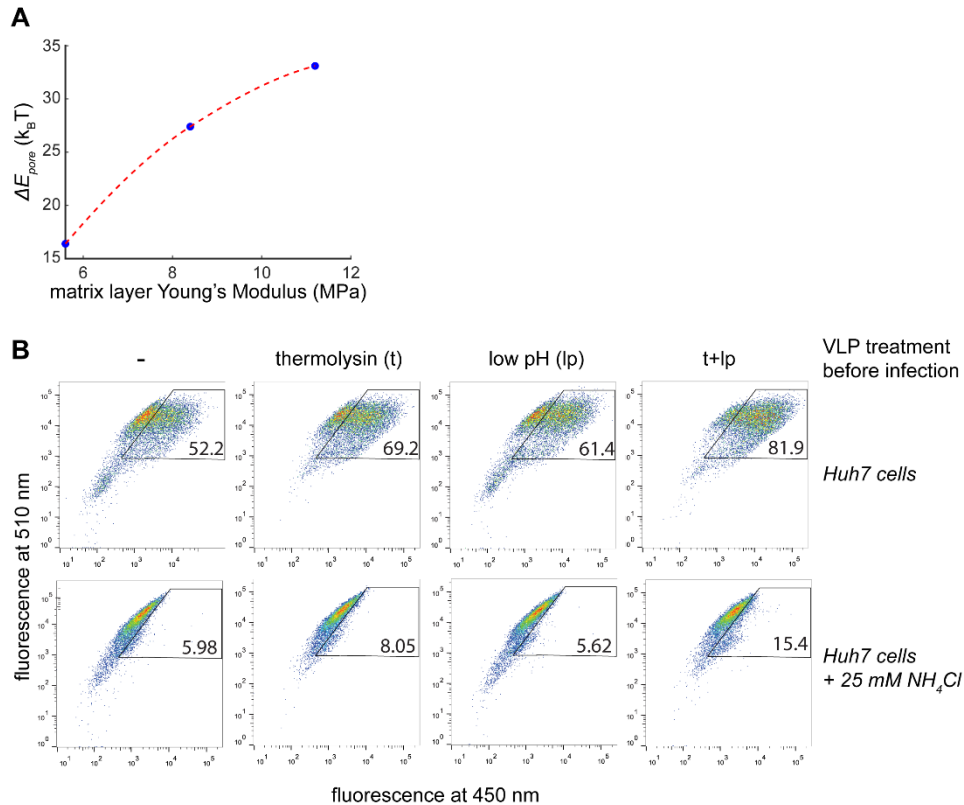
50 **Structural characterization of unpurified EBOV VLPs of different protein**
 51 **composition.** From top to bottom, the VLPs are composed of VP40, GP and the nucleocapsid
 52 (NC) proteins NP, VP24 and VP35; VP40 and GP; and VP40 alone. **(A)** Cross-sectional slices
 53 through tomograms showing filamentous VLPs at pH 7.4. **(B)** Near-to-surface slices of
 54 tomograms showing the top view of VLPs incubated at pH 7.4 and exhibiting the characteristic
 55 striations of the VP40 matrix (white arrows). **(C)** Cross-sectional slices through tomograms
 56 showing VLPs incubated at pH 4.5. No ordered VP40 matrix is visible adjacent to the VLP
 57 membrane as indicated by white arrowheads. Scalebars: 50 nm.



58

59 **Appendix Figure S4**

60 **Calibration of pHluorin fluorescence and decay times. (A)** Fluorescence intensity of HEK
 61 293T cells expressing pHluorin-VP40 measured at 488 nm as a function of pH. Cells were
 62 grown in cell culture media before exchanging the media with HNE buffer (10 mM HEPES, 100
 63 mM NaCl, 1 mM EDTA) at different pH. **(B)** pH characteristic decay times as found by fitting the
 64 pH levels to Eq. 3 of VLPs (red) and HEK 293T cells (blue) expressing pHluorin-VP40 and
 65 influenza M2 in increasing M2 levels. Filamentous VLPs 134±7 sec (n=154), spherical VLPs
 66 43±7 sec (n=66), cells expressing VP40 only 84±12 sec (n=44), cells expressing VP40 and M2
 67 at 1:0.002 molar ratio 71±11 sec (n=30), cells expressing VP40 and M2 at 1:0.02 molar ratio
 68 43±15 sec (n=28), cells expressing VP40 and M2 at 1:0.2 molar ratio 15±4 sec (n=26).



69

70 **Appendix Figure S5**

71 **Entry of Ebola BlaM-VLPs into Huh7 cells.** (A) Plot showing the dependence of the change in
 72 fusion pore formation energy between $u_0=38 \text{ k}_B T/\text{nm}^2$ to $u_0=0$ (ΔE_{pore}) on the matrix layer
 73 Young's modulus. Dotted lines serve as a guide to the eye. (B) FACS plots showing virus entry
 74 as measured by a fluorescence shift of infected cells from emission at 510 nm (no entry) to 450
 75 nm (entry). The top row indicates in vitro VLP treatments prior to infection including buffer
 76 control (-), thermolysin treatment, low pH treatment, and a combination of thermolysin and low
 77 pH. The first row of FACS data shows entry into Huh7 target cells, the second row shows entry
 78 into Huh7 cells treated with 25 mM ammonium chloride to neutralize acidic compartments and
 79 assess virus entry in the absence of acidification. FACS data are shown from one out of three
 80 repetitions, with 10000 cells measured per sample.